Available online at www.sciencedirect.com
ScienceDirect
Journal of Catalysis 245 (2007) 316–325
JOURNAL OF CATALYSIS
www.elsevier.com/locate/jcat

Catalytic oxidation of *n*-hexane on Mn-exchanged zeolites: Turnover rates, regioselectivity, and spatial constraints

Bi-Zeng Zhan [a], Björn Modén [a], Jihad Dakka [b], José G. Santiesteban [b], Enrique Iglesia [a,*]

[a] *Department of Chemical Engineering, University of California at Berkeley, 201 Gilman Hall, Berkeley, CA 94720, USA*
[b] *Corporate Strategic Research, ExxonMobil Research and Engineering Co., Route 22 East, Annandale, NJ 08801, USA*

Received 2 August 2006; revised 18 October 2006; accepted 21 October 2006

Available online 28 November 2006

Abstract

The effects of channel structure and spatial constraints on *n*-hexane oxidation rates and regioselectivity were examined on Mn cations within channels of acidic zeolites. Active Mn cations were placed at exchange sites within channels in 8-membered (ZSM-58), 10-membered (ZSM-5 and ZSM-57), and 12-membered ring (MOR) channels by sublimation of MnI_2. Synthesis rates for hexanols (ROH), hexanal/hexanones (R(–H)=O), and acids were proportional to hexylhydroperoxide (ROOH) concentrations on all Mn-zeolite catalysts, except Mn-ZSM-58, on which products formed exclusively via noncatalytic autoxidation because of restricted access to Mn cations present within small channels (0.36 nm). Catalytic decomposition of ROOH intermediates occurs on intrachannel Mn cations and is the kinetically relevant step in alkane oxidation. ROOH decomposition rate constants were 2.5, 1.4, and 0.41 mol (mol-Mn h)$^{-1}$ (mM-ROOH)$^{-1}$ on Mn-ZSM-5, Mn-ZSM-57, and Mn-MOR (403 K; 0.4 MPa O_2), respectively. Regioselectivity was influenced by the constrained environment around Mn cations, which increased terminal selectivities above the values predicted from the relative bond energies of methyl and methylene C–H bonds in *n*-hexane. Mn cations within 10-ring channels gave higher terminal selectivities (Mn-ZSM-5: 24%, $k_{prim}/k_{sec} = 0.42$; Mn-ZSM-57: 14%, $k_{prim}/k_{sec} = 0.22$) than those within 8-membered or 12-membered rings (Mn-MOR, Mn-ZSM-57: 8–10%, $k_{prim}/k_{sec} = 0.12$–0.14), because of restricted access in ZSM-58 and unconstrained transition states for C–H bond activation in MOR. Terminal selectivities decreased with increasing alkane conversion, because unselective noncatalytic autoxidation pathways prevail as ROOH concentrations concurrently increase. ROOH intermediates can be scavenged from the extracrystalline liquid phase using H-zeolites with accessible protons, which inhibit unselective noncatalytic reactions and maintain higher terminal selectivities as conversion increases, albeit with a concomitant decrease in the rate of oxidation steps also involving ROOH intermediates.

Keywords: *n*-Hexane oxidation; Terminal selectivity; Zeolite; Exchange; Sublimation

1. Introduction

The design of inorganic catalysts for selective oxidation of alkanes to alcohols, ketones, and acids using O_2 remains a formidable challenge. Enzymes with nonheme iron active centers (e.g., ω-hydroxylase) catalyze alkane oxidation with O_2 with high terminal selectivity [1], apparently because ligands near active centers favor specific docking of reactants at such active sites. Recent studies have tried to replicate these properties for nonbiological systems with modest success. Linear alkanes react with moderate terminal selectivities (~20%) on spatially constrained Mn(III) centers in metalloporphyrins [2]. Oxidation of *n*-hexane by iodosobenzene (PhIO) on 5,10,15,20-tetrakis (2′,4′,6′-triphenylphenyl)-porphyrinato-manganese(III) acetate [(MnTTPPP(OAc)] gives 19% 1-hexanol among alkanols, with a corresponding primary selectivity index (k_{prim}/k_{sec}) of 0.31 [3]. These k_{prim}/k_{sec} values are much greater than on Mn(III)-porphyrins with less constrained active centers ($k_{prim}/k_{sec} = 0.03$; 5,10,15,20-tetraphenyl-porphyrinato-manganese(III) acetate). Molecular simulations suggest that 2′,4′,6′-triphenylphenyl substituents on porphyrin macrocycles form a 0.4- to 0.5-nm pocket, which imposes constraints favoring selective oxygen insertion at terminal methyl groups [2]. Random C–H bond activation would give k_{prim}/k_{sec} values of unity (43% terminal selectivity for *n*-hexane), whereas relative C–H bond strengths and linear free

* Corresponding author. Fax: +1 510 642 4778.
E-mail addresses: iglesia@berkeley.edu, eiglesia@aol.com (E. Iglesia).

0021-9517/$ – see front matter © 2006 Published by Elsevier Inc.
doi:10.1016/j.jcat.2006.10.019

energy relations predict k_{prim}/k_{sec} values of ∼0.10 (∼7% terminal selectivity for *n*-hexane) [4].

Sterically hindered homogeneous 2,4-dichloro-3,5-dinitrobenzoic carboxylate Rh complexes gave some preferential terminal selectivity (31%) for carbene insertion into *n*-hexane ($k_{prim}/k_{sec} = 0.60$) [5]. Higher terminal selectivities have been reported for borylation reactions of alkanes. Bis(pinacolato)-diborane (B_2pin_2) or pinacolborane (HBpin) react with *n*-octane on Rh complexes with bulky ligands (Cp*Rh(η^4-C_6Me_6)) to give 65% yields of the terminal reaction product (*n*-octanyl-1-Bpin) [6].

Crystalline aluminosilicates contain cages and channels of varying size and shape, which can influence selectivity in catalytic reactions [7,8]. These zeolite materials also have negatively charged frameworks, which can be compensated for by redox-active cations [9,10] or porphyrin or phthalocyanine cationic complexes [11–14]. Framework substitutions can also introduce redox-active centers, as in the case of Co and Mn redox-active sites within microporous aluminophosphates (AlPO) [15,16]. Modest terminal selectivities have been reported for alkane oxidation with O_2 on these inorganic systems [17]. For example, terminal selectivities of 21% ($k_{prim}/k_{sec} = 0.54$) were measured for *n*-octane oxidation by O_2–H_2 mixtures on Fe/Pd-zeolite 5A; these k_{prim}/k_{sec} values increased (to 0.67) after selective titration of unconstrained sites at external surfaces with 2,2′-bipyridine [17]. The reaction products, however, could be removed only by dissolving the zeolite framework, because they cannot leave intracrystalline voids by diffusion through the 8-ring windows (∼0.4 nm) in zeolite A [17]. Unprecedented terminal selectivities were reported on MnAPO-18 and CoAPO-18 structures with small 8-ring windows (0.38 nm) [16]. Terminal selectivities as high as ∼65% ($k_{prim}/k_{sec} = 2.5$) were claimed for *n*-hexane (and *n*-octane) oxidation using O_2, with hexanoic acid as the predominant product; however, these findings have remained unconfirmed on catalysts with identical composition and structure [4,18]. Modest terminal selectivities were also reported for alkane oxidation with H_2O_2 on zeolites modified by redox-active cations. *n*-Octane reactions gave 45% terminal selectivity ($k_{prim}/k_{sec} = 1.6$) on Fe-ZSM-5 [19]. On vanadium silicalite (VS-2), *n*-hexane reactions with H_2O_2 gave contradictory results; one study reported 32% terminal selectivity ($k_{prim}/k_{sec} = 0.63$) [20], whereas another reported much lower values (11%; $k_{prim}/k_{sec} = 0.16$) [21].

A preference for oxygen insertion at terminal C–H bonds, despite their greater bond strength, appears to require steric effects arising from bulky ligands [2,5,6] or small channels [16,17]. Such preferences may reflect a specific mode of attachment of alkanes at redox-active sites [16], the inhibited termination of primary radicals [22], or the selective decomposition and regeneration of specific organoperoxide isomers constrained by the space surrounding active centers. Here we explore *n*-hexane–O_2 reactions on Mn cations present as exchanged species within zeolite channels of varying size and connectivity. In these systems, Mn redox-active sites decompose ROOH intermediates in kinetically relevant steps that occur within environments with varying degrees of spatial constraints.

2. Experimental

2.1. Synthesis and modification of catalysts

NH_4-mordenite (MOR) was obtained from Zeolyst (CBV 21A; $SiO_2/Al_2O_3 = 20$). NH_4-ZSM-5 (MFI) was obtained from ALSI-PENTA Zeolithe GmbH (SM-27; $SiO_2/Al_2O_3 = 24$). ZSM-58 (DDR) was prepared in its Na-form as described previously [23]; its organic template was removed by heating to 803 K at 0.167 K s^{-1} in flowing dry air (Praxair, UHP; 1.67 cm^3 s^{-1}) and holding at 803 K for 10 h. Its Na form was exchanged with NH_4^+ by stirring in 1.0 M NH_4NO_3 (Aldrich, 99.99+% in deionized water, 5 cm^3 (g-zeolite)$^{-1}$) for 3 h at ambient temperature, filtering, and washing the solids with deionized water. This exchange procedure was carried out three times. ZSM-57 (MFS) was prepared as the Na form as reported previously [24]. It was converted to its H form using the same procedures as for H-ZSM-58. The NH_4 form of each zeolite was converted to its H form by heating to 803 K at 0.167 K s^{-1} in flowing He (Praxair, UHP; 1.67 cm^3 s^{-1}) and holding for 4 h.

Mn^{2+} cations were exchanged onto H-zeolites using sublimation methods [25], because diffusion of charged Mn-oxo species in aqueous solutions is very slow within small- and medium-pore zeolites [26,27]. Zeolite samples were held within a glass ampoule (2 g) and treated at 573 K for 0.5 h in dynamic vacuum (∼1.3 × 10^{-2} Pa) to remove adsorbed species, cooled to ambient temperature, and finally mixed with anhydrous MnI_2 (Aldrich, 99.9%); the glass ampoule was sealed in vacuum, heated to 803 K at 0.167 K s^{-1}, and held at 803 K for 10 h. The samples were then dispersed in deionized water at 323 K, and the HI thus formed was removed by rinsing with hot deionized water (323 K). Mn-exchanged zeolites were heated in flowing dry air (Praxair, UHP; 1.67 cm^3 s^{-1}) to 393 K, held for 2 h, and then heated to 803 K at 0.167 K s^{-1} and held for another 2 h before catalytic and characterization tests.

2.2. Structural and chemical characterization

Micropore volumes were measured from N_2 uptakes at its normal boiling point (Autosorb 6, Quantachrome) after treating samples at 573 K in dynamic vacuum (∼4 Pa, 4 h). Isotopic exchange of D_2 with acidic and silanol OH groups was used to measure the number of OH groups remaining after exchange with Mn^{2+} [28]. Samples were treated in 1.67 cm^3 s^{-1} dry air (Praxair, UHP) within a quartz cell by heating to 803 K at 0.167 K s^{-1} and holding for 1 h. The samples were then cooled to ambient temperature and exposed to 5% D_2/Ar (Matheson; 0.67 cm^3 s^{-1}) while increasing the temperature to 803 K at 0.167 K s^{-1}. Intensities at 2–4 amu (H_2, HD, and D_2), 16–20 amu (water isotopomers), and 40 amu (Ar, internal standard) were measured by mass spectrometry (Orion Compact, MKS Instruments) at 12-s intervals.

Magic-angle spinning (MAS) ^{27}Al nuclear magnetic resonance (NMR) spectra were measured with a Bruker 500 spectrometer (11.7 T field) at 14 kHz after hydrating samples at ambient temperature to weaken quadrupole interactions that tend to broaden ^{27}Al NMR lines [26]. ^{27}Al spectra were acquired

with a 1.1-μs ($\pi/15$ flip angle) pulse width and a 1-s pulse delay and referenced to aqueous $Al(NO_3)_3$ (0 ppm). Infrared spectra were measured using a Mattson spectrometer (RS-10000) after dehydrating samples at 803 K in flowing He (Praxair, UHP; 1.67 $cm^3\ s^{-1}$) for 1 h; infrared spectra were acquired at 803 K in He with a 4-cm^{-1} resolution and 256 scans.

2.3. Catalytic rates and selectivities

n-Hexane (⩾99.0%, absolute, Fluka; 25 cm^3) oxidation rates and selectivities were measured in a shielded high-pressure glass reactor (Andrews Glass; 100 cm^3). Catalysts were transferred into the reactor immediately after treatment in dry air (Praxair, UHP) at 803 K for 2 h. 1,2-Dichlorobenzene (0.20 cm^3, 99.8%, Fisher Scientific) was used as an internal standard. The reaction unit was flushed three times by O_2 (Airgas, UHP), after which the pressure was increased to 0.3 MPa using O_2 at ambient temperature. The reactor temperature was raised to 403 K, which led to a final reactor pressure of 0.7 MPa (0.4 MPa O_2 and 0.3 MPa *n*-hexane); this O_2 pressure was maintained constant by adding O_2 periodically as it was consumed. Noncatalytic oxidation rates were measured under identical conditions but without adding a catalyst. Reactant and product concentrations were measured by periodically extracting a sample (∼0.50 cm^3) of clear liquid from the reactor.

2.4. Gas chromatographic analysis

The concentrations of reactants, products, and internal standard were measured by gas chromatography (Agilent 6890, with mass selective and flame ionization detectors) using a DB-WAX capillary column (60 m × 0.25 mm × 0.5 μm film; Agilent J&W Scientific). The oxidation products detected (3-hexanone, 2-hexanone, hexanal, 3-hexanol, 2-hexanol, 1-hexanol, acetic acid, propionic acid, butyric acid, valeric acid, and hexanoic acid) were identified by their MS fragmentation patterns and confirmed by chromatographic retention times measured for the pure compounds. Each sample was analyzed twice, before and after reaction with triphenylphosphine (Ph_3P; Fluka, ⩾98.5%), which converts hexylhydroperoxide isomers quantitatively to the corresponding alcohols [29–31]. Alcohols (ROH), ketones and aldehyde (R(–H)=O), and peroxides (ROOH) were measured from these two chromatograms by assuming that thermal decomposition of hexylhydroperoxides during chromatography leads to equimolar alcohol–ketone (or aldehyde) mixtures in underivatized samples. C_2–C_5 acids formed during reaction via oxidative C–C bond cleavage of ROH and R(–H)=O products; these are reported based on the number of *n*-hexane molecules appearing as a given product, taking into account that two shorter acids are formed when a ROH or R(–H)=O is cleaved. All rates and selectivities are reported based on the number of *n*-hexane molecules converted to each product.

3. Results and discussion

3.1. Exchange of Mn ions onto Brønsted acid sites

Table 1 shows compositions and micropore volumes for zeolite samples before and after Mn exchange. The measured Mn/Al ratios were similar to those in the starting MnI_2–H-

Table 1
Elemental analysis and pore volumes for Mn-zeolite catalysts

Entry	Zeolite structure	Channel/window size (nm)	Si/Al (atomic ratio)	Mn/Al[a] (atomic ratio)	Mn/Al_f[b] (atomic ratio)	Mn content (mmol g^{-1})	Micropore volume ($cm^3\ g^{-1}$)
1	H-MOR	0.65 × 0.70 0.34 × 0.48	10	–	–	–	0.206
2	Mn-MOR-3	0.65 × 0.70 0.34 × 0.48	10	0.020 (0.020)	–	0.029	0.163
3	Mn-MOR-2	0.65 × 0.70 0.34 × 0.48	10	0.040 (0.040)	–	0.060	0.164
4	Mn-MOR-1	0.65 × 0.70 0.34 × 0.48	10	0.088 (0.083)	0.17	0.093	0.165
5	H-ZSM-5	0.53 × 0.56 0.51 × 0.55	13	–	–	–	0.112
6	Mn-ZSM-5	0.53 × 0.56 0.51 × 0.55	13	0.088 (0.10)	0.14	0.10	0.105
7	H-ZSM-57	0.51 × 0.54	21	–	–	–	0.149
8	Mn-ZSM-57	0.51 × 0.54	21	0.12 (0.13)	–	0.13	0.139
9	H-ZSM-58	0.36 × 0.44	66	–	–	–	0.131
10	Mn-ZSM-58	0.36 × 0.44	66	0.47 (0.52)	0.47	0.11	0.131

[a] Mn/Al ratios were calculated using elemental analysis results (from Galbraith Laboratory); numbers in the parentheses reflect the Mn/Al molar ratio calculated from the MnI_2 and H-zeolite in the starting physical mixture.

[b] Framework Al (Al_f) measured from solid state ^{27}Al-NMR.

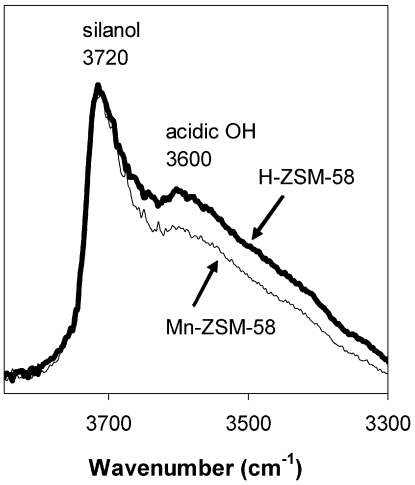

Fig. 1. Infrared spectra of H-ZSM-58 (—) and Mn-ZSM-58 (- - -). Samples were dehydrated in flowing He (1.67 $cm^3\ s^{-1}$) at 803 K for 1 h before recording spectra at 803 K in He.

zeolite physical mixtures, indicating that sublimation led to stoichiometric exchange for 12-ring, 10-ring, and 8-ring channels, because any unexchanged MnI_2 would have been removed during subsequent washing with water (323 K) or by sublimation during subsequent thermal treatment in air at 803 K for 2 h [27]. The Si/Al ratios in zeolites were unchanged by these synthesis protocols. N_2 adsorption uptakes indicated that Mn incorporation decreased micropore volumes slightly for all Mn/Al ratios on MOR (entries 1–4, Table 1). These changes were smaller for zeolites with higher Si/Al ratios (e.g., ZSM-57; entries 7 and 8 in Table 1); the micropore volume was unchanged by exchange for ZSM-58 (Si/Al = 66) (entries 9 and 10 in Table 1).

The extent of exchange and the possible extraction of some framework Al were probed by the intensity of the OH stretches in infrared spectra, by ^{27}Al NMR lines for tetrahedral and octahedral Al-species, and by D_2 exchange with OH groups remaining after MnI_2 sublimation. Fig. 1 shows that infrared bands for Brønsted acid centers (OH groups at Al centers) in H-ZSM-58 became less intense after contact with MnI_2(g) (Mn/Al = 0.47), indicating that MnI_2(g) can access internal zeolite regions even through 8-ring windows. Silanol bands at 3720 and ~3500 cm^{-1} interfered with those for acidic OH groups at 3600 cm^{-1} (because of the high Si/Al ratio of 66) [32,33], preventing accurate measurements of the number of O–H groups replaced by O–Mn using infrared spectroscopy. Therefore, isotopic exchange of OH groups with D_2(g) was used as an alternate method for this sample. Table 2 shows that 2.1 protons were removed per Mn^{2+} for Mn-ZSM-58 (column 4, Table 2), as expected from Mn^{2+} monomers bridging Al-exchange sites. OH/Al_f ratios were above unity (Al_f, framework Al measured by ^{27}Al-NMR; OH, measured by D_2 exchange) in both H-ZSM-58 and Mn-ZSM-58 (column 5 in Table 2) because of the large relative number of silanols at these high Si/Al ratios (66), consistent with infrared spectra (Fig. 1) and with similar previous reports on high-silica zeolites [32,33].

^{27}Al NMR did not detect extra-framework Al (Al_{oct}) in H-ZSM-58 or Mn-ZSM-58 (Fig. 2), indicating that dealumination did not occur during exchange protocols (Table 1). Al_{oct} species

Table 2
OH groups measured by D_2–OH and OH/Al_f by ^{27}Al NMR

	Mn/Al (molar ratio)	OH/Al[a] (molar ratio)	$OH_{consumed}/Mn$[b] (molar ratio)	OH/Al_f
H-ZSM-58	0	3.4	–	3.4
Mn-ZSM-58	0.47	2.4	2.1	2.4

[a] All OH groups (Brønsted and silanol) measured by D_2–OH exchange.
[b] $OH_{consumed}$ is the difference between Mn-zeolite and its H-form.

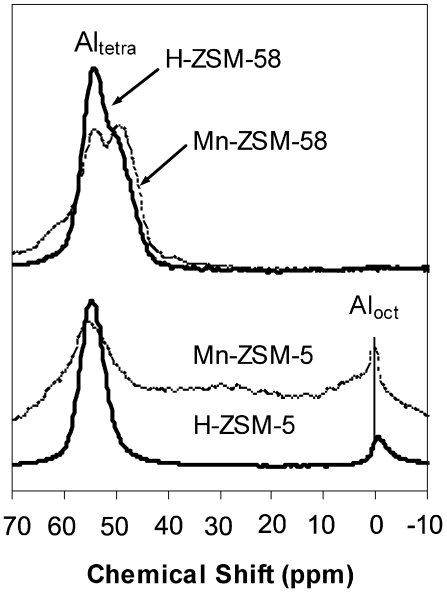

Fig. 2. Solid state MAS ^{27}Al NMR of zeolites before and after MnI_2 exchange. Framework tetrahedral Al: Al_{tetra}; extraframework octahedral Al: Al_{oct}.

were detected in Mn-ZSM-5 (39% of total Al; Fig. 2) and Mn-MOR (47% of total Al) samples with relatively low Si/Al ratios, suggesting that some significant dealumination occurred by HI formed in the sublimation, as also can be inferred from N_2 uptake measurements (Table 1).

3.2. Noncatalytic oxidation reactions of n-hexane

First, we provide *n*-hexane oxidation rates and selectivities without a catalyst as a benchmark for regioselectivity comparisons. *n*-Hexane reacted slowly with O_2 to form oxygenates at 403 K and 0.7 MPa total pressure, even without a catalyst (Fig. 3). Hexylhydroperoxide (ROOH) formation rates increased with time in the early stages of reaction (Fig. 3b). This induction period for ROH + R(–H)=O formation was longer than for ROOH formation (~3 h vs 1 h; Fig. 3a), consistent with the intermediate role of ROOH in the formation of products. Hexylhydroperoxides were the only products detected during the first 0.5 h (Fig. 3b), consistent with autoxidation pathways involving ROOH as the initial product,

$$RH + O_2 \rightarrow ROOH \rightarrow ROH + R(–H)=O \rightarrow \cdots. \quad (1)$$

Peroxide (e.g., *tert*-butylhydroperoxide) initiators eliminate these induction periods [34,35]. The terminal selectivity among all ROOH intermediates was 8.2% ($k_{prim}/k_{sec} = 0.12$) during this initial period, as would be expected given the relative

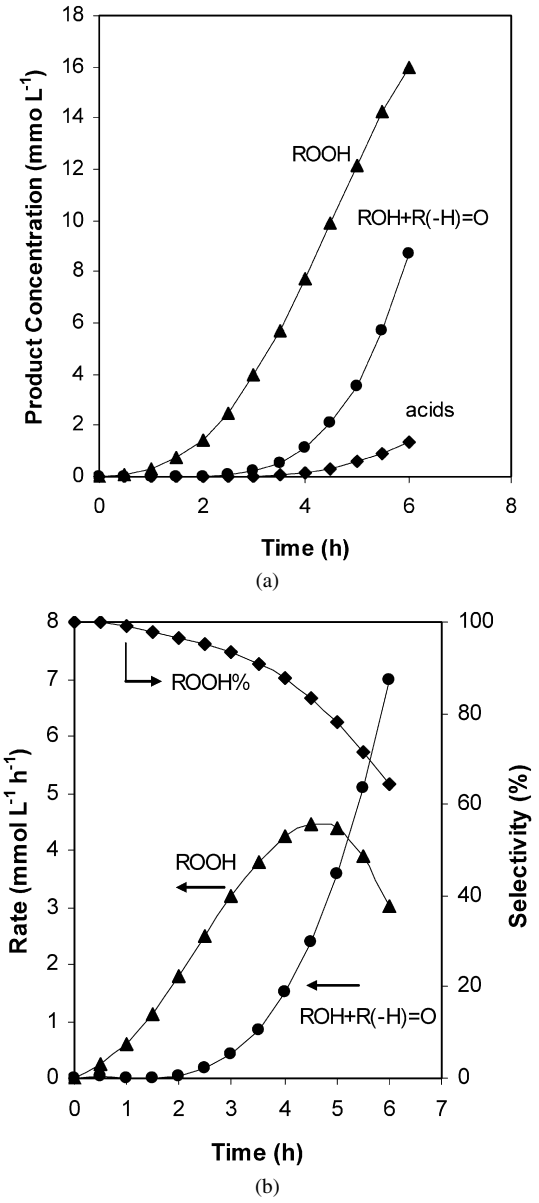

Fig. 3. Non-catalytic oxidation of *n*-hexane with O_2: (a) ROOH (▲), ROH + R(–H)=O (●), and acids (◆) including hexanoic acid and smaller acids formed via C–C bond cleavage; (b) r_{ROOH} (▲), $r_{ROH+R(-H)=O}$ (●), and ROOH selectivity (◆). Reaction conditions: 25 cm^3 *n*-hexane, 0.20 cm^3 dichlorobenzene, 403 K, and 0.7 MPa.

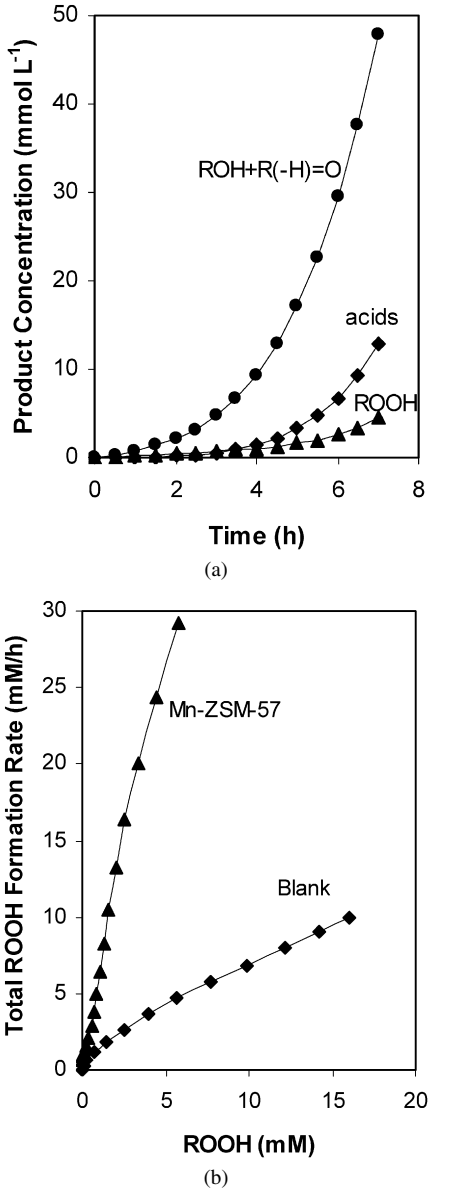

Fig. 4. *n*-Hexane oxidation on Mn-ZSM-57: (a) product concentrations: ROOH (▲), ROH + R(–H)=O (●), and acids (◆); (b) total ROOH formation rates (net ROOH measured + its products) vs lumped ROOH concentration along with blank (non-catalytic) reaction for comparison. Reaction conditions: 25 cm^3 *n*-hexane, 0.20 cm^3 dichlorobenzene, 1.00 g Mn-ZSM-57, 403 K, and 0.7 MPa.

abundance and energies of C–H bonds in *n*-hexane and linear free-energy treatments of chemical reaction rates (∼7%, $k_{prim}/k_{sec} = 0.10$) [4].

3.3. Catalytic oxidation of n-hexane on Mn-exchanged zeolites

Fig. 4 shows formation rates of ROOH and products [ROH, R(–H)=O, and acids] as a function of reaction time (and ROOH concentration) for *n*-hexane oxidation on Mn-ZSM-57. Mn-ZSM-57 gave lower ROOH concentrations and shorter induction periods for ROH + R(–H)=O formation than noncatalytic reactions (Fig. 4a vs Fig. 3a), because Mn sites provide catalytic routes for ROH + R(–H)=O formation from ROOH. These data (Fig. 4b) show that Mn-ZSM-57 also increased total ROOH formation rates (the sum of ROOH and its products) but to a lesser extent than ROOH decomposition rates, leading to lower prevalent ROOH concentrations than are present during non-catalytic autoxidation. Turnover rates for the synthesis of ROH, R(–H)=O, and acids were proportional to ROOH concentration (Fig. 5), consistent with the intermediate role of ROOH and with the identity and kinetic relevance of its decomposition steps, as shown earlier for alkane oxidation on MnAPO catalysts [4,34]. The kinetically relevant ROOH decomposition is catalyzed by redox-active Mn sites (Step **I** or **I′** in Scheme 1).

Product formation rates were proportional to ROOH concentrations on Mn-MOR and Mn-ZSM-5 as well (Fig. 5). Pseudo-first-order rate constants for ROOH decomposition to

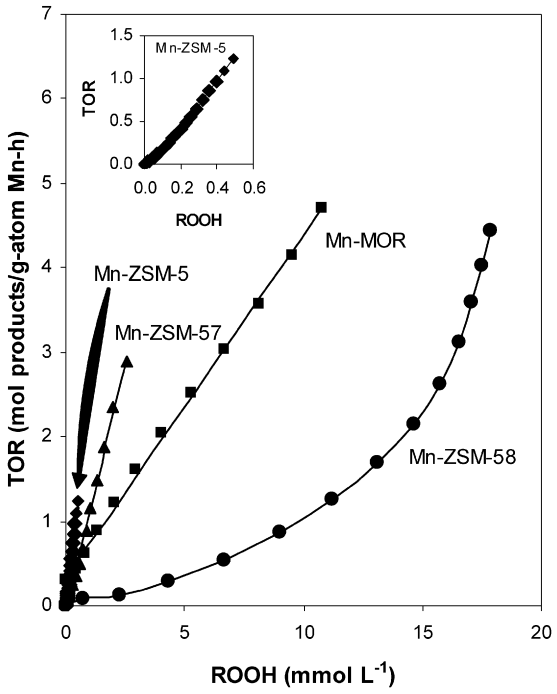

Fig. 5. Turnover rates (TOR) for combined formation of ROH, R(–H)=O, and acids on Mn sites vs lumped ROOH concentration: Mn-ZSM-58 (●), Mw-MOR (e.g., Mn-MOR-1 in Table 1) (■), Mn-ZSM-57 (▲), and Mn-ZSM-5 (◆). Reaction conditions: 25 cm^3 *n*-hexane, 0.20 cm^3 dichlorobenzene, 1.00 g Mn-zeolites, 403 K, and 0.7 MPa. Amplified profile for Mn-ZSM-5 is inserted in the left corner.

form ROH, R(–H)=O, and acids (from data in Fig. 5) were 2.5, 1.4, and 0.41 mol (g-atom-Mn h)$^{-1}$ (mM-ROOH)$^{-1}$ on 10-ring Mn-ZSM-5 and Mn-ZSM-57 catalysts and 12-ring Mn-MOR catalysts, respectively. The lower ROOH decomposition rates on Mn-MOR relative to those on Mn-ZSM-5 and Mn-ZSM-57 may reflect the presence of some Mn cations at sites within 8-ring channels inaccessible to ROOH [36,37]. These *n*-hexane oxidation rate constants are similar to those reported on MnAPO-5 and MnAPO-18 [0.31 and 0.38 mol (g-atom-Mn h)$^{-1}$ (mM-ROOH)$^{-1}$, respectively] at similar reaction conditions [4]. Product formation rates showed a larger than linear increase with ROOH concentration on 8-ring Mn-ZSM-58 (Fig. 5), a kinetic behavior characteristic of noncatalytic autoxidation pathways [35]. These effects of zeolite structure on *n*-hexane oxidation rates indicate that ROOH decomposition rates on Mn active centers are influenced by confining Mn redox-active sites within channels of varying size. Zeolites with 10-ring structures gave higher ROOH decomposition rates and lower ROOH concentration than 8-ring and 12-ring zeolites (Fig. 5).

The effects of spatial constraints on regioselectivity were probed by measuring terminal oxidation selectivities at low ROOH concentrations (short reaction times, <0.5 h). These conditions minimize unselective noncatalytic autoxidation pathways, because these processes depend more sensitively on ROOH concentration than catalytic pathways. Table 3 gives initial terminal selectivities for Mn-zeolites with different channel/window sizes and for noncatalytic reactions. All catalysts except Mn-ZSM-58 demonstrated terminal oxidation selectivities greater than those for noncatalytic pathways, suggesting that spatial constraints influence the position of oxygen insertion and increase selectivity toward the activation of stronger C–H bonds in terminal CH_3 groups via reactions with Mn-bound reactive species (Scheme 1). Terminal selectivities (and k_{prim}/k_{sec} ratios) reached a maximum for 10-ring channels (Table 3) but were much lower than those reported on 8-ring (0.38 × 0.38 nm windows) MeAPO-18 catalysts (up to 65%; $k_{prim}/k_{sec} = 2.5$) [16]. Terminal selectivities on 8-ring zeolites (ZSM-58: 0.36 × 0.44 nm; 8.4% or $k_{prim}/k_{sec} = 0.12$) resemble those for noncatalytic autoxidation (8.2%, or

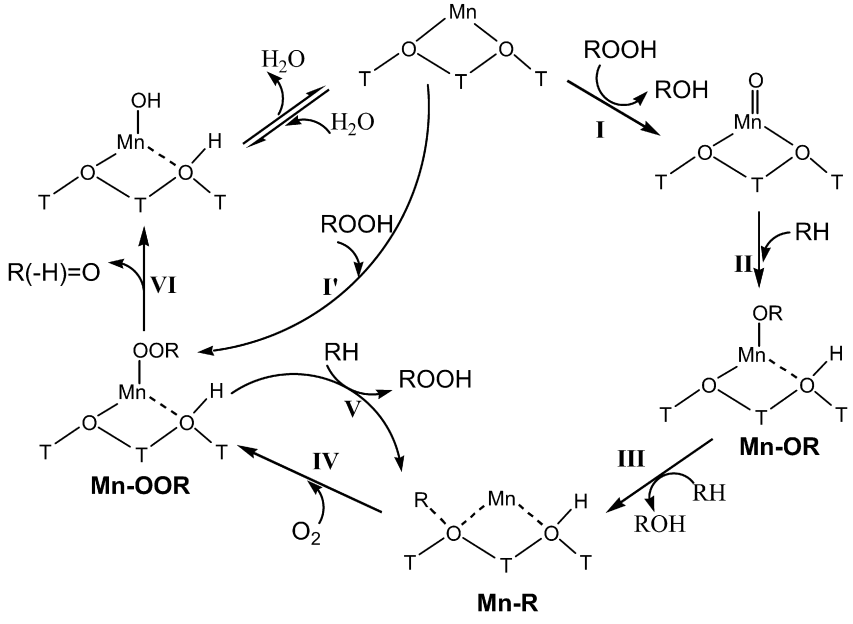

Scheme 1. Proposed ROOH decomposition mechanism on zeolite-confined Mn sites. ROOH = hexylhydroperoxides, ROH = hexanol, R(–H)=O = hexanone and hexanal; Mn–OOR, Mn–OR, and Mn–R are Mn-bound reactive intermediates.

Table 3
Initial terminal selectivity (within 0.5 h) of *n*-hexane oxidation on Mn-zeolites compared to non-catalytic pathways (without a catalyst)[a]

	ZSM-58	ZSM-5	ZSM-57	MOR	Without catalyst
Open windows (nm)	0.36 × 0.44	0.53 × 0.56	0.51 × 0.54	0.65 × 0.70	–
D_i[b]/d_{max}[c] (nm)	0.760/0.359	0.630/0.464	0.675/0.531	0.664/0.639	–
Initial terminal selectivity (%)	8.4	24	14	9.5	8.2
Primary selectivity index (k_{prim}/k_{sec})	0.12	0.42	0.22	0.14	0.12

[a] 25 cm^3 *n*-hexane, 0.20 cm^3 dichlorobenzene, 1.00 g Mn-zeolites, 403 K, and 0.7 MPa.
[b] Maximum included sphere diameter D_i.
[c] Maximum free sphere diameters d_{max}.

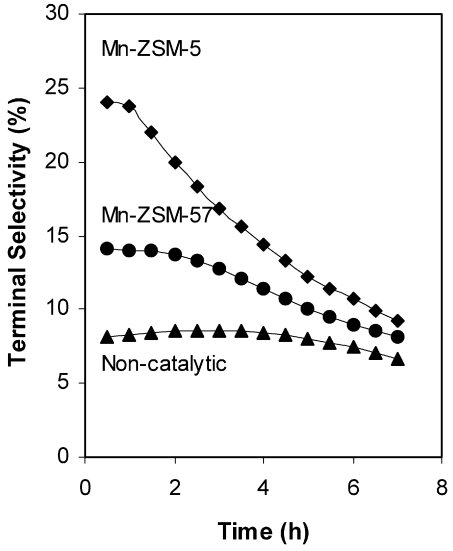

Fig. 6. Terminal selectivities for *n*-hexane oxidation vs reaction time: noncatalytic oxidation (▲), Mn-ZSM-57 (●), and Mn-ZSM-5 (◆). Reaction conditions: 25 cm^3 *n*-hexane, 0.20 cm^3 dichlorobenzene, 1.00 g Mn zeolites, 403 K, and 0.7 MPa.

$k_{prim}/k_{sec} = 0.12$); these data are consistent with previous reports that the 8-ring channels in ZSM-58 are inaccessible to small alkanes [38,39]. The 12-ring zeolites gave only slightly higher terminal selectivities than those for noncatalytic pathways (MOR: 0.65 × 0.70 nm; 9.5% or $k_{prim}/k_{sec} = 0.14$), because their large channels do not introduce spatial constraints that disfavor the activation of the weaker secondary C–H bonds.

Terminal selectivities on Mn cations within 10-ring zeolites (ZSM-57: 0.54 nm; 14% or $k_{prim}/k_{sec} = 0.22$; and ZSM-5: 0.56 nm; 24% or $k_{prim}/k_{sec} = 0.42$) were significantly higher than for noncatalytic pathways, but decreased with increasing reaction time (or ROOH concentration; Fig. 6), because unselective noncatalytic oxidation pathways prevail as ROOH concentrations increase. Thus, high terminal selectivity requires predominant contributions from catalytic pathways on Mn sites contained within microporous channels (such as 10-ring zeolites), which provide the required spatial constraints on catalytic steps (Scheme 1). In what follows, we examine the potential effects of Brønsted acid sites, present in all Mn-exchanged zeolites (Tables 1 and 2), on ROOH-mediated oxidation pathways. We also explore the influence of ROOH concentration on terminal oxidation selectivity for these zeolite structures.

3.4. Reaction pathways and elementary steps in n-hexane oxidation catalyzed by Mn zeolites

Brønsted acid sites catalyze ROOH decomposition via intramolecular rearrangements that form ROH and R(–H)=O without radical chains [40,41]. Cyclohexyl hydroperoxide decomposition rates increased markedly when Na^+ cations were replaced by H^+ on Y zeolite [40]. Infrared bands for cyclohexyl hydroperoxide (1367 cm^{-1}) were detected during cyclohexane photooxidation on Na-Y but not on H-Y, because cyclohexyl hydroperoxide decomposed rapidly on H^+ sites [40]. Thus, acidic OH groups can inhibit the accumulation of peroxide intermediates in the liquid phase as the reaction proceeds. In fact, ROOH was not detected even after 44 h during *n*-hexane oxidation on H-MOR at conditions leading to substantial ROOH formation even for noncatalytic reactions (16 mM or 1% conversion after 6 h). The absence of ROOH during *n*-hexane oxidation on H-MOR is in contrast to its detectable presence when Mn-MOR is used, because ROOH is regenerated on Mn active sites via a subcycle within the catalytic sequence (steps **IV** and **V**, Scheme 1) [4,34]. H-MOR scavenges ROOH intermediates, as also occurs for 10-ring zeolites (H-ZSM-57 and H-ZSM-5). Thus, volumetric *n*-hexane oxidation rates (~3×10^{-10} mol L^{-1} s^{-1}; see the slope in Fig. 7) on H-MOR reflect noncatalytic ROOH formation rates via direct reactions of RH with O_2 [e.g., Eq. (1)] without ROOH-mediated autoxidation propagation cycles. In contrast, 8-ring windows in H-ZSM-58 (0.36 × 0.44 nm) prevent access to intrachannel H^+ sites by RH or ROOH [38,39], a requirement for ROOH decomposition. Thus, H-ZSM-58 cannot scavenge ROOH intermediates, and, consequently, ROOH decomposition rate constants on H-ZSM-58 and Mn-ZSM-58 resemble those for noncatalytic autoxidation reactions of *n*-hexane (Fig. 8).

The role of H^+ sites within 10-ring and 12-ring zeolite channels as ROOH scavengers was confirmed by reacting *n*-hexane-O_2 mixtures on Mn-ZSM-5 for a prespecified period, during which ROOH concentrations increased and terminal selectivity concurrently decreased, and then adding H-ZSM-5 (Fig. 9) to scavenge ROOH molecules already formed. ROOH concentrations decreased immediately (from 0.02 to 0.005 mM) on the addition of H-ZSM-5 (0.1 g) to a reacting mixture containing Mn-ZSM-5 (1.0 g) after 0.05% *n*-hexane conversion (Fig. 9b). The initial terminal selectivity was ~24% (or $k_{prim}/k_{sec} = 0.42$) in these experiments and decreased to ~16% ($k_{prim}/k_{sec} = 0.25$) after 0.05% *n*-hexane conversion. It remained constant at this value (up to 0.13% conversion) after

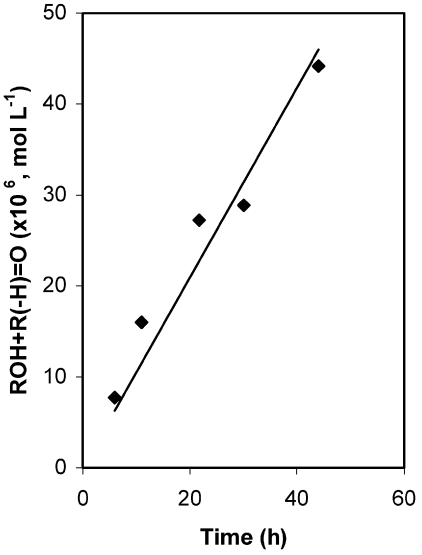

Fig. 7. n-Hexane oxidation on H-MOR. Reaction conditions: 25 cm^3 n-hexane, 0.20 cm^3 dichlorobenzene, 0.5 g H-MOR, 403 K, and 0.7 MPa.

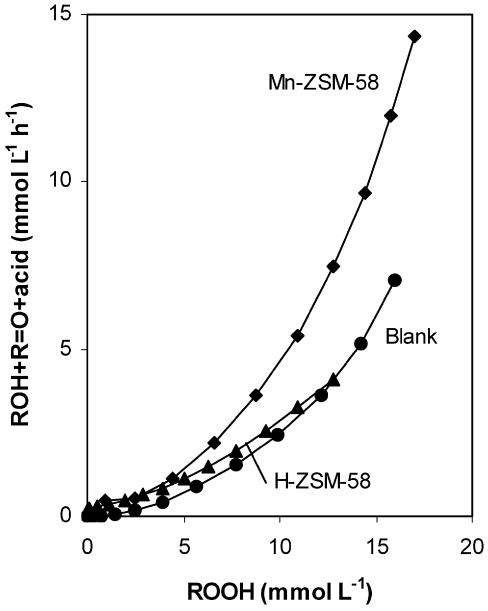

Fig. 8. ROH + R(–H)=O formation rates vs [ROOH] on Mn-ZSM-58 (1.00 g, ◆), H-ZSM-58 (1.00 g, ▲), and blank (non-catalytic, ●). Reaction conditions: 25 cm^3 n-hexane, 0.20 cm^3 dichlorobenzene, 403 K, and 0.7 MPa.

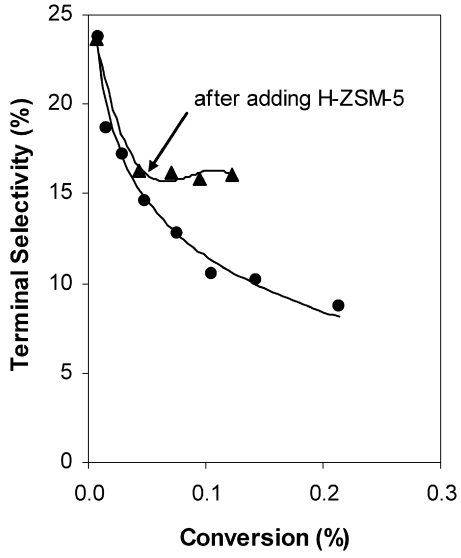

(a)

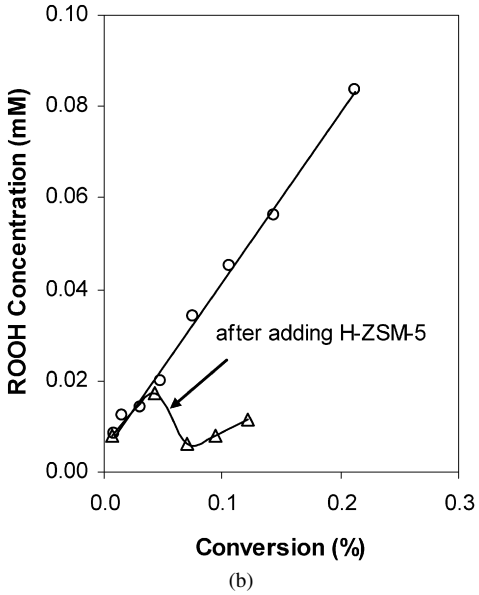

(b)

Fig. 9. Terminal selectivity and measured ROOH concentration during n-hexane oxidation on Mn-ZSM-5: 1.00 g Mn-ZSM-5 (●, ○) and 1.00 g Mn-ZSM-5 + 0.10 g H-ZSM-5 (▲, △). Reaction conditions: 25 cm^3 n-hexane, 0.20 cm^3 dichlorobenzene, 403 K, and 0.7 MPa; for the control experiment, 0.10 g H-ZSM-5 was added after n-hexane oxidation on 1.00 g Mn-ZSM-5 for 1 h.

introducing H-ZSM-5, which scavenged ROOH and minimized contributions from unselective noncatalytic pathways. These terminal selectivities were much greater than on Mn-ZSM-5 alone (∼10% or $k_{prim}/k_{sec} = 0.15$) at this higher conversion level (0.13%; Fig. 9a). Thus, H-ZSM-5 scavengers maintain high terminal selectivities by decreasing ROOH concentrations and concomitant noncatalytic routes, albeit with a concurrent marked decrease in catalytic alkane oxidation rates, which are proportional to the prevalent ROOH concentration.

Kinetic and isotopic studies have shown that alkane reactions with O_2 on MnAPO-5 proceed via heterogeneous chain-transfer pathways limited by organoperoxide decomposition on Mn redox-active sites [34]. Product formation rates were proportional to ROOH concentrations, as we also report here for n-hexane oxidation on Mn active sites exchanged onto 10- and 12-ring zeolites (Fig. 5). These rates are comparable to those measured for n-hexane oxidation on MnAPO-18 and MnAPO-5 under similar reaction conditions [4], as discussed above. These data and the structural resemblance between Mn-zeolites and MnAPO materials indicate that n-hexane oxidation proceeds via similar catalytic sequences (Scheme 1). ROOH decomposes on Mn sites to form either Mn-bound RO species (Mn–OR; steps **I** and **II** in Scheme 1) or Mn-bound ROO intermediates (Mn–OOR; step **I′** in Scheme 1). Mn–OR then reacts with RH to give ROH and Mn-bound alkyl species (Mn–R; step **III**), which in turn react with O_2 to reform ROO on Mn centers

(Mn–OOR; step **IV**). Mn–OOR decomposes to form aldehyde or ketone [R(–H)=O] to regenerate Mn sites (step **VI**) or reacts with RH to form another ROOH molecule (step **V**). Steps **IV** and **V** provide a subcycle within the catalytic sequence, forming additional ROOH molecules that maintain the ROOH concentration and propagate the catalytic cycle. These branching pathways are unavailable during ROOH decomposition on H-zeolites because of their inability to regenerate ROOH [40,41], as discussed above (Fig. 5 vs Fig. 7).

In this oxidation sequence, the position of oxygen insertion can be influenced by spatial constraints that orient alkanes as they approach Mn-bound reactive intermediates so as to form terminal 1-RO, 1-R, and 1-ROOH species (via steps **II**, **III**, and **V**) preferentially over species containing O atoms at weaker secondary C–H bonds. These steps reflect spatial constraints on ROOH decomposition and some preference for the activation of terminal C–H bonds by Mn-bound organic species involved in the heterogeneous chain-transfer processes of Scheme 1 rather than the direct terminal C–H bond activation by unoccupied Mn redox-active sites.

Foster et al. have tabulated the largest cavities (the diameter of the largest inscribed sphere, D_i) and apertures (the maximum free sphere diameter, d_{max}) for all known zeolite frameworks using triangulation methods [42]. Among ZSM-5, ZSM-57, and MOR, which allow diffusion of RH and ROOH to access confined Mn sites, ZSM-5 has the smallest cavity (0.630 nm D_i) and aperture (0.464 nm d_{max}), compared with 0.675 nm D_i and 0.531 nm d_{max}; for ZSM-57 and 0.664 nm D_i and 0.639 nm d_{max} for MOR (Table 3). Thus, ZSM-5 provides more severe spatial constraints and the regioselective pathways that favor terminal oxidation selectivity (24% or $k_{prim}/k_{sec} = 0.42$) (Table 3).

4. Conclusion

Infrared spectroscopy, ^{27}Al solid-state NMR, N_2 physisorption, and $D_2(g)$ exchange with remaining OH groups in zeolites have indicated that Mn cations are stoichiometrically exchanged onto 8-, 10- and 12-membered ring H-zeolites ZSM-58, ZSM-5, ZSM-57, and MOR through the sublimation of MnI_2. The nature of ROOH-mediated kinetically relevant steps in alkane oxidation on Mn zeolites (and MnAPO materials) determines that terminal selectivity for linear alkane-O_2 oxidation is strongly influenced by three factors: ROOH regeneration, spatial constraints around Mn cations, and competitive oxidation between heterogeneous and unselective noncatalytic pathways. Oxidation rates are first order in ROOH concentration on Mn-ZSM-5, Mn-ZSM-57, and Mn-MOR, with suitable channel sizes allowing access of RH and ROOH to confined Mn sites, and larger than first order in ROOH on Mn-ZSM-58, a kinetic behavior typical of noncatalytic autoxidation pathways, because its 8-ring windows are inaccessible to both RH and ROOH. The ROOH decomposition rate constant on Mn-ZSM-5 [2.5 mol (g-atom-Mn h)$^{-1}$ (mM-ROOH)$^{-1}$] is higher than that on Mn-ZSM-57 [1.4] and on Mn-MOR [0.41]. The 10-ring zeolite channels preferentially orient terminal C–H over secondary C–H bonds in reactions with Mn-bound reactive species, leading to enhanced terminal selectivities. In particular, Mn-ZSM-5 gives a three-fold increase in initial terminal selectivity compared with unselective noncatalytic pathways (24% or $k_{prim}/k_{sec} = 0.42$ vs 8.2% or $k_{prim}/k_{sec} = 0.12$). Terminal selectivities decrease with increasing reaction time (or ROOH concentration) due to the increasing contribution from unselective autoxidation, which is more sensitive to the ROOH concentration than heterogeneous catalytic steps. Sustained high terminal selectivity was attained by the addition of 10-ring and 12-ring H-zeolites, which scavenge ROOH intermediates; terminal selectivity was maintained with increasing conversion, albeit at comparably lower conversion rates.

Acknowledgments

The authors acknowledge financial support and permission to publish these results from ExxonMobil Research and Engineering Co.

References

[1] M. Hamberg, B. Samuelsson, I. Bjorkhem, H. Danielsson, in: O. Hayaishi (Ed.), Oxygenases in Fatty Acid and Steroid Metabolism, Academic, New York, 1974, p. 29.
[2] B.R. Cook, T.J. Reinert, K.S. Suslick, J. Am. Chem. Soc. 108 (1986) 7281.
[3] Defined as the ratio of primary to secondary products normalized by the number of each type of C–H bonds.
[4] B. Moden, B.Z. Zhan, J. Dakka, J.G. Santiesteban, E. Iglesia, J. Phys. Chem. B (2006), in press.
[5] A. Demonceau, A.F. Noels, P. Teyssie, A.J. Hubert, J. Mol. Catal. 49 (1988) L13.
[6] H.Y. Chen, S. Schlecht, T.C. Semple, J.F. Hartwig, Science 287 (2000) 1995.
[7] A. Corma, Chem. Rev. 95 (1995) 559.
[8] R. Szostak, Molecular Sieves: Principles of Synthesis and Identification, Van Nostrand Reinhold, New York, 1989.
[9] B. Moden, P. Da Costa, B. Fonfe, D.K. Lee, E. Iglesia, J. Catal. 209 (2002) 75.
[10] T. Waku, J.A. Biscardi, E. Iglesia, Chem. Commun. (2003) 1764.
[11] B.Z. Zhan, X.Y. Li, Chem. Commun. (1998) 349.
[12] V.Y. Zakharov, O.M. Zakharova, B.V. Romanovskii, R.E. Mardaleishvili, React. Kinet. Catal. Lett. 6 (1997) 133.
[13] P.P. Knopsgerrits, D. Devos, F. Thibaultstarzyk, P.A. Jacobs, Nature 369 (1994) 543.
[14] K.J. Balkus, M. Eissa, R. Levado, J. Am. Chem. Soc. 117 (1995) 10753.
[15] B. Moden, L. Oliviero, J. Dakka, J.G. Santiesteban, E. Iglesia, J. Phys. Chem. B 108 (2004) 5552.
[16] J.M. Thomas, R. Raja, G. Sankar, R.G. Bell, Nature 398 (1999) 227.
[17] N. Herron, C.A. Tolman, J. Am. Chem. Soc. 109 (1987) 2837.
[18] P. Tian, L. Xu, T. Huang, P. Xie, Z.-M. Liu, Chem. J. Chin. Univ. 23 (2002) 656.
[19] N. Herron, New J. Chem. 13 (1989) 761.
[20] T. Tatsumi, Y. Watanabe, Y. Hirasawa, J. Tsuchiya, Res. Chem. Intermed. 24 (1998) 529.
[21] P. Rao, A.V. Ramaswamy, J. Chem. Soc. Chem. Commun. (1992) 1245.
[22] J.A. Labinger, J. Mol. Catal. A Chem. 220 (2004) 27.
[23] E.W. Valyocsik, US Paternt 4,698,217 (1987).
[24] J. Dakka, M. Mertens, Patent WO 03,029,144 (2003).
[25] H.S. Lacheen, E. Iglesia, J. Phys. Chem. B 110 (2006) 5462.
[26] R.W. Borry, Y.H. Kim, A. Huffsmith, J.A. Reimer, E. Iglesia, J. Phys. Chem. B 103 (1999) 5787.
[27] Q. Sun, W.M.H. Sachtler, Appl. Catal. B Environ. 42 (2003) 393.
[28] J.A. Biscardi, G.D. Meitzner, E. Iglesia, J. Catal. 179 (1998) 192.
[29] G.B. Shulpin, D. Attanasio, L. Suber, J. Catal. 142 (1993) 147.

[30] D.L. Vanoppen, D.E. Devos, M.J. Genet, P.G. Rouxhet, P.A. Jacobs, Angew. Chem. Int. Ed. 34 (1995) 560.
[31] B.Z. Zhan, M.A. White, J.A. Pincock, K.N. Robertson, T.S. Cameron, T.K. Sham, Canad. J. Chem. 81 (2003) 764.
[32] G.L. Woolery, L.B. Alemany, R.M. Dessau, A.W. Chester, Zeolites 6 (1986) 14.
[33] M. Hunger, S. Ernst, S. Steuernagel, J. Weitkamp, Microporous Mater. 6 (1996) 349.
[34] B. Moden, B.Z. Zhan, J. Dakka, J.G. Santiesteban, E. Iglesia, J. Catal. 239 (2006) 390.
[35] R.A. Sheldon, J.K. Kochi, Metal-Catalyzed Oxidation of Organic Compounds, Academic Press, New York, 1981.
[36] J. Dědeček, B. Wichterlová, J. Phys. Chem. B 103 (1999) 1462.
[37] J. Dědeček, D. Kaucký, B. Wichterlová, Microporous Mesoporous Mater. 35–36 (2000) 483.
[38] W. Zhu, F. Kapteijn, J.A. Moulijn, Chem. Commun. (1999) 2453.
[39] W. Zhu, F. Kapteijn, J.A. Moulijn, M.C. den Exter, J.C. Jansen, Langmuir 16 (2000) 3322.
[40] H. Sun, F. Blatter, H. Frei, J. Am. Chem. Soc. 118 (1996) 6873.
[41] R.A. Sheldon, The Chemistry of Functional Groups, Peroxides, Wiley, New York, 1983.
[42] M.D. Foster, I. Rivin, M.M.J. Treacy, O.D. Friedrichs, Microporous Mesoporous Mater. 90 (2006) 32.